DOE/MC/29061-96/C0665

CONF-9510109--41

Manifold Methods for Methane Combustion

Author:

B. Yang
S. B. Pope

RECEIVED
APR 09 1996
OSTI

1

MASTER

Disclaimer

Manifold Methods for Methane Combustion

B. Yang (byang@mae.cornell.edu, 607-255-8270)
S. B. Pope (pope@mae.cornell.edu, 607-255-4314)
Upson Hall
Cornell University
Ithaca, NY 14853

1. Introduction

Great progresses have been made in combustion research, especially, the computation of laminar flames [1,2,3,4] and the probability density function (PDF) method in turbulent combustion [5,6,7]. For one-dimensional laminar flames, by considering the transport mechanism, the detailed chemical kinetic mechanism and the interactions between these two basic processes, today it is a routine matter to calculate flame velocities, extinction, ignition, temperature, and species distributions from the governing equations. Results are in good agreement with those obtained from experiments [8,9]. However, for turbulent combustion, because of the complexities of turbulent flow, chemical reactions, and the interaction between them, in the foreseeable future, it is impossible to calculate the combustion flow field by directly integrating the basic governing equations. So averaging and modeling are necessary in turbulent combustion studies. Averaging, on one hand, simplifies turbulent combustion calculations, on the other hand, it introduces the infamous closure problems, especially the closure problem with chemical reaction terms. Since in PDF calculations of turbulent combustion, the averages of the chemical reaction terms can be calculated, PDF methods overcome the closure problem with the reaction terms. It has been shown that the PDF method is a most promising method to calculate turbulent combustion [6]. PDF methods have been successfully employed to calculate laboratory turbulent flames: they can predict phenomena such as super equilibrium radical levels, and local extinction [7]. Because of these advantages, PDF methods are becoming used increasingly in industry combustor codes.

Although PDF methods have shown great promise in studying turbulent combustion, there is still a challenge to be overcome - coupling the detailed description of the turbulent combustion flow field provided by PDF methods with detailed chemical kinetic mechanisms. Suppose that $\phi(t)$ represents the composition of a particle in a PDF calculation of turbulent combustion. Then we need to calculate the increment in composition $\Delta\phi(t)$ over a time step Δt. In principal, this can be done by directly integrating the ordinary differential equations stemming from the detailed kinetic mechanism. But in practice, since a typical combustion system involves dozens of chemical species and hundreds of chemical reactions, and we need to do such integrations on the order of 10^9 times, the direct numerical integration of the equations would require huge amount of supercomputer time (several hundred days) and thus make it impossible in practical use. So simplifications of detailed kinetic mechanisms have been made in the

past in order to reduce the demand of computer time. Results from the calculations of simplified chemistry are tabulated as functions of a few variables. Then these tables are used in turbulent combustion calculations.

There are basically two different ways of doing the simplification of detailed chemistry: the reduced mechanism method [10,11,12] and the intrinsic low-dimensional manifold (ILDM) method [13]. For the reduced mechanism method, the simplification made to the detailed chemistry is achieved by the introducing steady-state assumptions for some species, usually the intermediate species, and the partial equilibrium assumptions for particular reactions. The reduced mechanism method has been employed in laminar flame calculations and in turbulent combustion calculations [7,14]. It has several disadvantages because of it's fundamental philosophy. For the reduced mechanism method, one needs to know in advance what species are in steady-state, and what reactions are in partial equilibrium. Reduced mechanism systems are derived manually from the given detailed chemistry. For different fuel/oxidizer systems, or even for the same fuel/oxidizer system under different conditions, different reduced mechanisms should be used. Thus it requires a considerable amount of human time and labor to develop such systems. Assumptions of partial-equilibrium and steady-state used in the reduced mechanism method are only valid in particular reaction ranges. Also the accuracy cannot be given and controlled.

The manifold method is based on a more intrinsic study of the chemical reaction process happening in combustion [13]. As it is observed, there is a wide range of time scales for chemical reactions, from 10^{-9} second to seconds. Fast reactions, or reactions with small time scales, quickly bring composition points down to attracting manifolds. Then composition points move along on manifolds. By assuming that the movement of the composition point away from manifolds to be zero, detailed chemistry can be simplified. The manifold method overcomes the drawbacks of the reduced mechanism method. It requires no preliminary knowledge of which chemical species are in steady-state and which chemical reactions are in partial equilibrium. The only given assumption is the dimension of the manifold. The manifold method has been successfully used in both laminar flames and turbulent combustion studies [7,14]. In these studies, a manifold with fixed dimension, for example, two dimensions, has been considered. The results from manifold calculations are tabulated in a pre-processing stage. Then the method of table-look-up is used in PDF calculations. There are still some difficulties and inconveniences:

- In general, it is not straightforward to parametrize the manifold.

- In different regions of the composition space, manifolds of different dimension are appropriate.

- The table generation (which is not fully automated) must be performed for each set of conditions of interest (fuel, pressure, equivalence ratio, etc.).

- The whole of the manifold is (wastefully) tabulated since it is not known *a priori* which regions are needed.

So a more efficient way is needed which can preserve the virtues of the manifold method and overcome these difficulties and inconveniences.

4

2. Objectives

Our objective is to develop a new method which can be used to study realistic chemistry in methane combustion with NO_x mechanism. The realistic chemistry used is a simplification to a more detailed chemistry based on the manifold method. The accuracy of the simplified chemistry can be controlled, and it is determined by the interaction between the transport process and the chemical reaction process, and the phenomena we are interested in.

3. Approaches

The new method developed here is called the "tree method." The basic idea of it is quite simple. It is shown in the following picture. As the PDF or partially stirred reactor (PaSR) calculations are performed, an unstructured table is generated, containing N pairs of compositions and their corresponding increments, $\{\phi^{(n)}, \Delta\phi^{(n)}, n = 1, 2, ..., N\}$. The table is stored in a tree structure that is initially empty (N=0). For each particle on each time step in the PDF or PaSR calculations, the increment $\Delta\phi$ is sought based on the particle's composition ϕ. The tree is searched for an entry $\phi^{(n)}$ close to ϕ. If one exists, then $\Delta\phi^{(n)}$ is used to approximate $\Delta\phi$. If a sufficiently close table entry does not exist, then $\Delta\phi$ is computed by the direct integration of equations from detailed chemistry, and the result is added to the table.

There are several key problems needed to be solved in the development of this new method. First, in the beginning stage, a partially stirred reactor needed to be constructed to provide composition particles and a tool for testing the new method. Second, for a complex chemistry like that of methane flames, the number of the pairs in the unstructured table
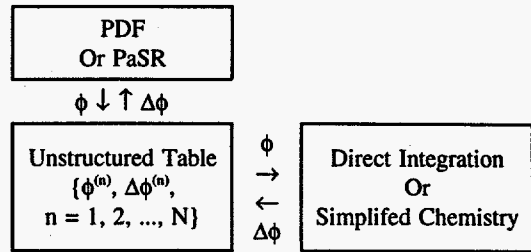

Figure 1. A Schematic Illustration of the Method

may be very large for a required accuracy. So the way to search for a close entry $\phi^{(n)}$ to ϕ should be efficient. Third, we need to develop a method to couple reaction and mixing.

3.1 Partially Stirred Reactor

A partially stirred reactor, as shown in the following picture, has M particles, or L = M/2 pairs of particles. For convenience, all particles in the PaSR are initialized to the complete combustion condition (for methane-air combustion, only N_2, H_2O, and CO_2 exist under the complete combustion condition) at the beginning. After time step Δt, there are $m_{out} = L\Delta t/\tau_{res}$ pairs of particles flow out of the reactor, where τ_{res} is the residence time. Randomly choose $m_{pair} = L\Delta t/\tau_{pair}$ pairs of particle and put them in the candidate pile. Here τ_{pair} is a time scale of pairing. There are $m_{in} = m_{out}$ pairs of particles flowing into the PaSR, and they pair randomly with the particles in the candidate pile. Then mixing occurs between pairs of particles.

3.2 The Method for Generating An Unstructured Table

The ideas of the method for generating an unstructured table are the followings. The composition space is covered by cells. There are two kinds of cells - the coarse cells (of different sizes) and the fine cells (of different sizes). There is a single composition point
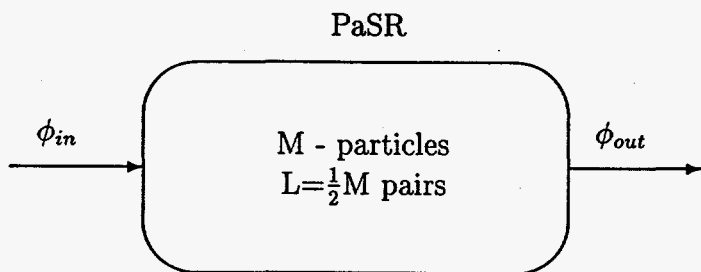
Figure 2. A Partially Stirred Reactor

that represents a cell. For a fine cell, all increments of compositions of points in the cell are accurately represented by the increment of the representative cell point. For a given composition point, the cells are searched based on the indexes of the components of the composition. These indexes are determined by the expected accuracy. If the indexes match the indexes of a composition point in the unstructured table, then the value of the increment of this point is returned. Otherwise, the given composition point is added to the table and the increment is calculated.

3.3 Coupling Mixing and Reaction in Intrinsic Low-Dimensional Manifolds

As it will be shown in the section of accomplishments and applications, particles away from manifolds quickly relax to manifolds due to the fast chemical reactions. So we base our calculations on the particles on manifolds. The following section describes the method, for a given particle, how to find the closest manifold point of it.

3.3.1 The Closest Manifold Point

Let the composition of a particle be $\phi = \{Y_1, Y_2, ..., Y_{ns}, h\}^T$, where Y_i, i = 1, 2, ..., n_s, is the mass fraction of species i, n_s is the number of species, and h is the specific

enthalpy. Let $n = n_s + 1$ be the dimension of ϕ. The evolution of ϕ is determined by the equation:

$$\frac{d\phi}{dt} = S, \qquad (1)$$

where S is the source term due to chemical reactions. For a given particle $\phi^{(0)}$, the closest manifold point $\phi^{(m)}$ is defined as follows. At the manifold point $\phi^{(m)}$, let

$$W = \begin{bmatrix} W^s \\ W^f \end{bmatrix}$$

be the matrix such that, $\hat{\phi}^s = W^s\phi$ is in the slow subspace, and $\hat{\phi}^f = W^f\phi$ is in the fast subspace [13,14] (these subspaces are defined in terms of the eigenvalues λ_i and the eigenvectors of the Jacobian matrix J, $J_{\alpha,\beta} = \partial S_\alpha(\phi)/\partial\phi_\beta$). The dimension of the slow subspace, m_s, is determined by the given flow time scale τ^*, which means that the eigenvalues of the slow subspace, $\lambda_i > -1/\tau^*$, i = 1, 2, ..., m_s. The dimension of the fast subspace is $m_f = n - m_s$. Suppose that W^e is a matrix determining the element conservation, then the closest manifold point $\phi^{(m)}$ is determined by solving the following problem:

Minimize the 2-norm of $\phi^{(m)} - \phi^{(0)}$, subject to the following conditions:

$$W^e(\phi^{(m)} - \phi^{(0)}) = 0, \qquad (2)$$

$$W^f S(\phi^{(m)}) = 0, \qquad (3)$$

$$\phi_i \geq 0, \ i = 1, 2, ..., n_s. \qquad (4)$$

These equations are solved by the iteration method. Let $\phi^{(i)}$ be the estimate of $\phi^{(m)}$ after the i-th iteration, the next iteration is

$$\phi^{(m)} \approx \phi^{(i+1)} = \phi^{(i)} + \delta\phi^{(i)} \equiv \phi^{(0)} + \Delta\phi^{(i)}.$$

With W evaluated at $\phi^{(i)}$, linearize Eq. 3 around $\phi^{(i)}$, write the equations in terms of $\Delta\phi^{(i)}$, Eqs. 2 and 3 become

$$W^e\Delta\phi^{(i)} = 0, \tag{5}$$

$$[W^f J]\Delta\phi^{(i)} = W^f\{J(\phi^{(i)} - \phi^{(0)}) - S(\phi^{(i)})\}. \tag{6}$$

Eqs. 5 and 6 are underdetermined. Generally, they are solved by the singular value decomposition method to get a minimum norm solution [15]. If a solution with negative mass fractions is found (in violation of conditions Eq. 4) then, we use the quadratic programming method [16,17] to get the minimum norm solution for Eqs. 5 and 6 under constraints (4).

3.3.2 Coupling Mixing and Reaction in Manifolds

This section describes how the coupling of mixing and reactions are treated to get the value of $\phi^{(0)}(t + \Delta t)$ for a given particle, $\phi^{(0)}(t)$. For ease of exposition, we use eigenvector basis vectors, in practical calculations, orthonormal bases for the subspaces are used.

At the beginning of the time step (from $t = 0$ to $t = \Delta t$), $\phi^{(0)}$ is close to the manifold: any departure of $\phi^{(0)}$ from the manifold is due to manifold curvature and the non-zero time step Δt. Denote the pairing particle of $\phi^{(0)}$ by $\phi_p^{(0)}$, perform the mixing:

$$\frac{d\phi^{(0)}}{dt} = (\phi_p^{(0)})/\tau_{mix}, \tag{7}$$

$$\frac{d\phi_p^{(0)}}{dt} = (\phi^{(0)} - \phi_p^{(0)})/\tau_{mix}, \tag{8}$$

where τ_{mix} is the mixing time scale. Solving Eqs. 7 and 8, we can get $\phi_{mix}^{(0)}(t+\Delta t)$ due to the mixing. This value is used to define the "mixing vector," F:

$$F \equiv \left[\phi_{mix}^{(0)}(t + \Delta t) - \phi^{(0)}\right]/\Delta t. \tag{9}$$

Let $\phi^{(m)}$ represent the closest manifold point to $\phi^{(0)}$. At $\phi^{(m)}$, calculate the projection matrix P,

$$P = \begin{bmatrix} P^s \\ P^c \\ P^f \end{bmatrix} \tag{10}$$

such that for any vector x

$$Px = \begin{bmatrix} \hat{x}^s \\ \hat{x}^c \\ \hat{x}^f \end{bmatrix} \tag{11}$$

where $\hat{x}^s$, $\hat{x}^c$, $\hat{x}^f$ are the components of x in the eigenvector bases of the "slow reactive," "conserved," and "fast reactive" subspaces. The equation coupling reaction and mixing is,

$$\frac{d\phi}{dt} = S(\phi) + F. \tag{12}$$

Linearize it about $\phi^{(m)}$,

$$\frac{d}{dt}\delta\phi = S^{(m)} + J\delta\phi + F, \tag{13}$$

7

where

$$\delta\phi \equiv \phi - \phi^{(m)}, \qquad (14)$$

$$S^{(m)} = S(\phi^{(m)}), \qquad (15)$$

and J is the Jacobian matrix,

$$J_{\alpha\beta} = \left[\frac{\partial S_\alpha(\phi)}{\partial\phi_\beta}\right]_{\phi^{(m)}}. \qquad (16)$$

Transform Eq. 12 by premultiplying it by P:

$$P\frac{d}{dt}\delta\phi = \frac{d}{dt}P\delta\phi =$$

$$\frac{d}{dt}\begin{bmatrix}\delta\hat{\phi}^s \\ \delta\hat{\phi}^c \\ \delta\hat{\phi}^f\end{bmatrix} = \begin{bmatrix}\hat{S}^m \\ 0 \\ 0\end{bmatrix} + \begin{bmatrix}\Lambda^s \\ 0 \\ \Lambda^f\end{bmatrix}\begin{bmatrix}\delta\hat{\phi}^s \\ \delta\hat{\phi}^c \\ \delta\hat{\phi}^f\end{bmatrix} + \begin{bmatrix}\hat{F}^s \\ \hat{F}^c \\ \hat{F}^f\end{bmatrix}. \qquad (17)$$

Note that the "conserved" components of $S^{(m)}$ and Λ are zero, by virtue of the conservation properties. The "fast" component of $S^{(m)}$ is zero by definition of the manifold.

For the "slow" and "conserved" components, Eq. 17 is to be integrated for a time step Δt from the initial condition,

$$\delta\phi(0) = \phi^{(0)} - \phi^{(m)}. \qquad (18)$$

The "fast" components are set to

$$\delta\hat{\phi}^f(\Delta t) = 0, \qquad (19)$$

so that the final result $\phi(\Delta t)$ is close to the manifold (i.e., it has no component in the fast subspace at $\phi^{(m)}$).

For the conserved component we have,

$$\frac{d}{dt}\delta\hat{\phi}^c = F^c, \qquad (20)$$

and so the solution is

$$\begin{aligned}\delta\hat{\phi}^c(\Delta t) &= \delta\hat{\phi}^c(0) + \hat{F}^c\Delta t \\ &= P^c\{(\phi^{(0)} - \phi^{(m)}) + (\phi^{(1)} - \phi^{(0)})\} \quad (21)\\ &= P^c\{\phi^{(1)} - \phi^{(0)}\}.\end{aligned}$$

The second step follows from the definition of F, and the third from the constraint that $P\phi^{(m)} = P\phi^{(0)}$. Thus, as expected, the conserved components in mixing are unaffected by reactions.

For a slow reactive component α, Eq. 17 is

$$\frac{d}{dt}\delta\hat{\phi}^s_\alpha = \hat{S}^{(m)}_\alpha + \hat{F}^s_\alpha + \lambda^s_\alpha\delta\hat{\phi}^s_\alpha. \qquad (22)$$

This has the analytic solution

$$\delta\hat{\phi}^s_\alpha(\Delta t) = a_\alpha\delta\hat{\phi}^s_\alpha(0) + b_\alpha\left[\hat{S}^m_\alpha + \hat{F}^s_\alpha\right], \qquad (23)$$

where

$$a_\alpha = e^{\lambda^s_\alpha\Delta t}, \qquad (24)$$

$$b_\alpha = (e^{\lambda^s_\alpha\Delta t} - 1)/\lambda^s_\alpha, \qquad (25)$$

For positive λ^s_α, the approximate solution,

$$\delta\hat{\phi}_\alpha^s(\Delta t) = \delta\hat{\phi}_\alpha^s(0) + \Delta t\left[\hat{S}_\alpha^m + \hat{F}_\alpha^s\right], \quad (26)$$

is used. This is corresponding to $a_\alpha = 1$, $b_\alpha = \Delta t$.

For a given Δt, whatever basis is used for the slow subspace, because Eq. 13 is linear, the solution can be written as,

$$\delta\hat{\phi}_\alpha^s(\Delta t) = A\delta\hat{\phi}_\alpha^s(0) + B\left[\hat{S}_\alpha^m + \hat{F}_\alpha^s\right], \quad (27)$$

In the eigenvector basis, $A = \text{diag}\{a_\alpha\}$, $B = \text{diag}\{b_\alpha\}$.

Let ϕ^R be the exact solution to

$$\frac{d\phi}{dt} = S(\phi), \quad (28)$$

from initial condition $\phi^{(m)}$, integrated for a time Δt, and define

$$\Delta\phi^R = \phi^{(R)} - \phi^{(m)}, \quad \Delta\hat{\phi}^R = P^s\Delta\phi^R. \quad (29)$$

Observe that the solution to the linearized system Eq. 27 for the same case is

$$(\Delta\hat{\phi}^R)_{\text{linearized}} = B\hat{S}^{(m)}, \quad (30)$$

(see Eq. 27). It is preferable to use the exact result. Hence Eq. 27 can be replaced by

$$\delta\hat{\phi}^s(\Delta t) = \Delta\hat{\phi}^R + A\delta\hat{\phi}^s(0) + B\hat{F}^s. \quad (31)$$

Let

$$P^{-1} = Q = [Q^s\ Q^c\ Q^f]. \quad (32)$$

Then the final result is

$$\phi(t + \Delta t) = \phi^{(m)} + \delta\phi(\Delta t) = \phi^{(m)} + P^{-1}\begin{bmatrix} \delta\hat{\phi}^s(\Delta t) \\ \delta\hat{\phi}^c(\Delta t) \\ 0 \end{bmatrix}$$

$$= \phi^{(m)} + Q^s\delta\hat{\phi}^s(\Delta t) + Q^c\delta\hat{\phi}^c(\Delta t). \quad (33)$$

4. Project Description

The work of this 2-year project is divided into the following parts:

1. Design a partially stirred reactor to provide sample points and integrate the governing equations of mixing and reaction simultaneously,

2. Introduce a method to treat chemical reactions and perform the coupling of mixing and reaction,

3. Find an efficient way of tabulation,

4. Perform tests to determine the accuracies and parameters used by the method,

5. Apply the new method to PDF calculations of turbulent methane combustions.

At the present stage, as discussed in Part 3, most work on Parts 1-3 has been done. We have a partially stirred reactor and a code to do the direct integration of the governing equations of mixing and reactions. The method to treat chemical reactions and perform the coupling of mixing and reaction was discussed in Section 3.3.2. The method is based on the manifold method, and the closest manifold point is used to do the mixing and reaction. The tabulation method is described

9

in Section 3.2. In order to determine the accuracies and parameters, we need to do some tests: PaSR tests - both for single particle and multiple particles (say 100 particles), using direct numerical integration; tests of the coupling model of mixing and reaction to measure errors and determine quantities used in tabulation; tests of tabulation, given a required accuracy, determine the cell-size criterion.

5. Accomplishments and Applications

The chemical kinetic mechanism used in calculations is shown in Table 1. It does not include the NO_x chemistry at the present.

In PaSR calculations, the incoming particles to the PaSR are methane/air mixtures at stoichiometric condition. The particles in the PaSR are initialized to the complete combustion - only CO_2, H_2O, and N_2 exist. Particles in the partially stirred reactor are arranged in pairs. Suppose that i'th and (i+1)'th particles are of a pair, the evolution of the particles are determined according to the following governing equations:

$$\frac{d\phi^{(i)}}{dt} = S + (\phi^{(i+1)} - \phi^{(i)})/\tau_{mix}, \quad (34)$$

$$\frac{d\phi^{(i+1)}}{dt} = S + (\phi^{(i)} - \phi^{(i+1)})/\tau_{mix}, \quad (35)$$

here S is the source term due to chemical reactions. In calculations, the mixing time scale $\tau_{mix} = 10^{-4}$ second, the pairing time scale $\tau_{pair} = 10^{-4}$ second, the residence time scale $\tau_{res} = 10^{-3}$ second. There are 100 particles in the partially stirred reactor, the time

step $\Delta t = 6 \times 10^{-5}$ second, the pressure is 1 atmosphere.

From direct integrations of Eqs. 34 and 35, the changes of the average mass fractions as functions of time are shown in Figs. 3-6. It can be seen that after about four residence times, the particles in the PaSR reach a statistically steady condition. For the first particle in the PaSR, the change of the mass fraction of water is plotted in Fig. 7. One interesting thing to note is that it reaches zero at time step 72, which means that this particle flow out of the PaSR at time step 72, corresponding to time = 4.32×10^{-3} second.

From the PaSR calculations, we have an ensemble of particles. Investigations have been done to study the chemical process which relaxes the particles to manifolds. Randomly choose particles from the PaSR calculations, plot the distances of particles from the corresponding manifold points, d, and the dimensions of the manifolds, m. They are illustrated in Figs. 8-13. In these figures, the solid lines represent the distances, and the dashed lines represent the dimensions. The figures show that the particles quickly relax to the corresponding manifolds. The typical time scale of such a relaxation process is on the order of 10^{-4} second, which is much smaller than a typical mixing process which has a time scale on the order of 10^{-3} second. So it would be a good assumption to assume that processes occur on manifolds.

The closest manifold points are calculated for the particles of the ensemble from calculations of the partially stirred reactor. The time scale τ^* equals 10^{-4} second. Fig. 14 shows the number of particles as a function of the dimensions of manifolds. One can see that most points are concentrated on low dimensional manifolds.

Table 1. Chemical Kinetic Mechanism*

No.	Reaction	A_n	n	E_n
1	H + O2 = OH + O	1.59E+17	-0.927	16874.
2	O + H2 = OH + H	3.87E+04	2.70	6262.
3	OH + H2 = H2O + H	2.16E+08	1.51	3430.
4	OH + OH = O + H2O	2.10E+08	1.40	-397.
5	H + H + M = H2 + M	6.40E+17	-1.0	0.
6	H + OH + M = H2O + M	8.40E+21	-2.00	0.
7	H + O2 + M = HO2 + M	7.00E+17	-0.80	0.
8	HO2 + H = OH + OH	1.50E+14	0.0	1004.
9	HO2 + H = H2 + O2	2.50E+13	0.0	693.
10	HO2 + O = O2 + OH	2.00E+13	0.0	0.
11	HO2 + OH = H2O + O2	6.02E+13	0.0	0.
12	H2O2 + M = OH + OH + M	1.00E+17	0.0	45411.
13	CO + OH = CO2 + H	1.51E+07	1.3	-758.
14	CO + O + M = CO2 + M	3.01E+14	0.0	3011.
15	HCO + H = H2 + CO	7.23E+13	0.0	0.
16	HCO + O = OH + CO	3.00E+13	0.0	0.
17	HCO + OH = H2O + CO	1.00E+14	0.0	0.
18	HCO + O2 = HO2 + CO	4.20E+12	0.0	0.
19	HCO + M = H + CO + M	1.86E+17	-1.0	16993.
20	CH2O + H = HCO + H2	1.26E+08	1.62	2175.
22	CH2O + O = HCO + OH	3.50E+13	0.0	3513.
23	CH20 + OH = HCO + H2O	7.23E+05	2.46	-970.
24	CH20 + O2 = HCO + HO2	1.00E+14	0.0	39914.
25	CH20 + CH3 = HCO + CH4	8.91E-13	7.40	-956.
26	CH20 + M = HCO + H + M	5.00E+16	0.0	76482.
27	CH3 + O = CH20 + H	8.43E+13	0.0	0.
28	CH3 + OH = CH20 + H2	8.00E+12	0.0	0.
29	CH3 + O2 = CH3O + O	4.30E+13	0.0	30808.
30	CH3 + O2 = CH2O + OH	5.20E+13	0.0	34895.
31	CH3 + HO2 = CH3O + OH	2.28E+13	0.0	0.
32	CH3 + HCO = CH4 + CO	3.20E+11	0.50	0.
33	CH4 + H = CH3 + H2	7.80E+06	2.11	7744.
34	CH4 + O = CH3 + OH	1.90E+09	1.44	8676.
35	CH4 + O2 = CH3 + HO2	5.60E+12	0.0	55999.
36	CH4 + OH = CH3 + H2O	1.50E+06	2.13	2438.
37	CH4 + HO2 = CH3 + H2O2	4.60E+12	0.0	17997.
38	CH3O + H = CH2O + H2	2.00E+13	0.0	0.
39	CH3O + OH = CH2O + H2O	5.00E+12	0.0	0.
40	CH3O + O2 = CH2O + HO2	4.28E-13	7.60	-3528.
41	CH30 + M = CH20 + H + M	1.00E+14	0.0	25096.

* Rate constants are in the form $k_n = A_n T^n \exp[-E_n/(\hat{R}T)]$, here $\hat{R}$ is the universal gas constant. Units are moles, cubic centimeters, seconds, Kelvins, and kJ/mole.

The complex tabulation method was tested for a simple function on a domain. This method was also used to tabulate the particles from the ensemble of PaSR calculations. It worked well for both cases. Further tests are needed.

Compared with the reduced mechanism method, the manifold method, and the tabulation method used before, the new method overcomes the drawbacks of the reduced mechanism method and preserves the advantages of the manifold method. The difficulties and inconveniences with the manifold method no longer exist in the new method because the dimensions of manifolds can be changed, the table is unstructured so that the manifolds do not have to be parametrized, the table is generated in situ as the PDF calculations is in progress so only the required regions are tabulated. Accuracy is achieved by specifying the size of the cell, which can be controlled. With all these advantages and it's high flexibilities, the new method will be a valuable toll for turbulent combustion calculations under various conditions.

6. Future Activities

In the future, we will test the method of coupling mixing and reaction against direct numerical integrations, determine the errors and the quantities that will be used in tabulation. Single particle calculation will be used to determine the effect of cell size on accuracy and storage in calculations using the tabulation method. The chemical kinetic mechanism will include NO_x chemistry.

Once we have all the information about accuracies, and control quantities, the new method will be applied to PaSR calculations to determine the overall performance. Finally, it will be implemented it to PDF calculations of turbulent methane combustion.

References

1. Smooke, M. D., Solution of Boundary-Stabilized Premixed Laminar Flames by Boundary Value Methods. *Journal of Computational Physics*, 48: 72-105, 1982.

2. Smooke, M. D., Error Estimate for the Modified Newton Method With Applications to the Solution of Nonlinear, Two-Point Boundary Value Problems. *Journal of Optimization Theory and Application*, Vol. 39, No. 4, pp. 489-511, 1983.

3. Smooke, M. D., Miller, J. A., and Kee, R. J., Solution of Premixed and Counterflow Diffusion Flame Problems by Adaptive Boundary Value Method. In *Numerical Boundary Value ODEs*, U. M. Ascher and R. D. Russell Eds., Birkhauser, Basel, 1985.

4. Dixon-Lewis, G., David, T., Gaskell, P. H., Fukutani, S., Jinno, H., Miller, J. A., Kee, R. J., Smooke, M. D., Peters, N., Effelsberg, E., Warnatz, J., and Behrendt, F., Calculation of the Structure and Extinction Limit of a Methane-Air Counterflow Diffusion Flame in the Forward Stagnation Region of a Porous Cylinder. *Twentieth Symposium (International) on Combustion*, The Combustion Institute, 1984, pp. 1893-1904.

5. Pope, S. B., PDF Methods for Turbulent Reactive Flows, *Progress in Energy and Combustion Science*, 11, 119-192, 1985.

6. Pope, S. B., Computations of Turbulent Combustion: Progress and Challenges. *Twenty-Third Symposium (International) on Combustion*, The Combustion Institute, 1990, pp. 591-612.

7. Norris, A. T., Pope, S. B., Modeling of Extinction in Turbulent Diffusion Flames by the Velocity-Dissipation-Composition PDF Method, *Combustion and Flame*, 100, 211-220 (1995).

8. Smooke, M. D., Crump, J., Seshadri, K., Giovangigli, V., Comparison Between Experimental Measurements and Numerical Calculations of the Structure of Counterflow, Diluted, Methane-Air, Premixed Flames. *Twenty-Third Symposium (International) on Combustion*, The Combustion Institute, 1990, pp. 463-470.

9. Smooke, M. D., Puri, I. K., Seshadri, K., A Comparison Between Numerical Calculations and Experimental Measurements of the Structure of a Counterflow Diffusion Flame Burning Diluted Methane in Diluted Air. *Twenty-First Symposium (International) on Combustion*, The Combustion Institute, 1986, pp. 1783-1792.

10. Peters, N., Numerical and Asymptotic Analysis of Systematically Reduced Reaction Schemes for Hydrocarbon Flames. In *Numerical Simulation of Combustion Phenomena*, Lecture Notes in Physics, 241, pp. 90-109, 1985.

11. Smooke, M. D. (Ed.), *Reduced Kinetic Mechanisms and Asymptotic Approximations for Methane-Air Flames*, Lecture Notes in Physics, Springer-Verlag, 1991, Vol. 384.

12. Peters, N., Rogg, B. (Eds.), *Reduced Kinetic Mechanisms for Applications in Combustion Systems*, Lecture Notes in Physics, Springer-Verlag, 1993.

13. Maas, U., Pope, S. B., Simplifying Chemical Kinetics: Intrinsic Low-Dimensional Manifold in Composition Space, *Combustion and Flame*, 88, 239-264 (1992).

14. Maas, U., Pope, S. B., Laminar Flame Calculations Using Simplified Chemical Kinetics Based on Intrinsic Low-Dimensional Manifolds, *Twenty-Fifth Symposium (International) on Combustion*, The Combustion Institute, Pittsburgh, 1994, pp. 1349-1356.

15. Golub, G. H., Van Loan, C. F., *Matrix Computations*, 2nd ed., John Hopkins University Press, Baltimore, 1989.

16. Coleman, T. F., A Reflective Newton Method for Minimizing a Quadratic Function Subject to Bounds on Some of the Variables. Cornell Theory Center, Cornell University, 1992.

17. Land, A. H., Fortran Codes for Mathematical Programming: Linear, Quadratic and Discrete. John Wiley & Sons, New York, 1972.
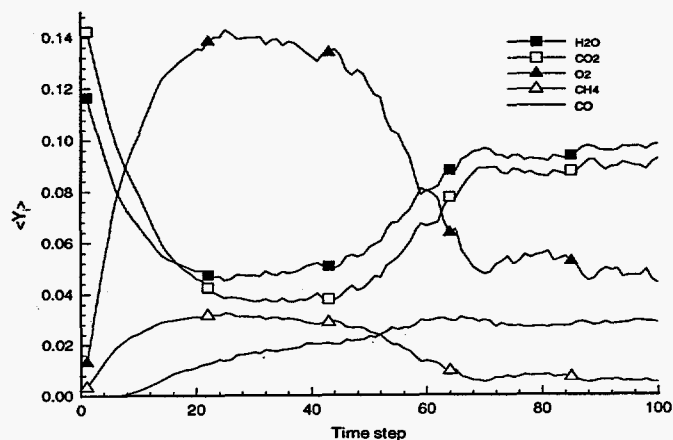
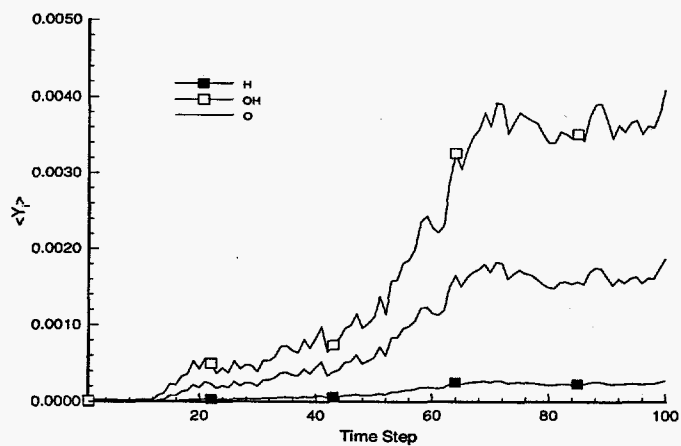**Figure 3. Average Mass Fractions of H_2O, CO_2, CH_4, CO as Functions of Time**

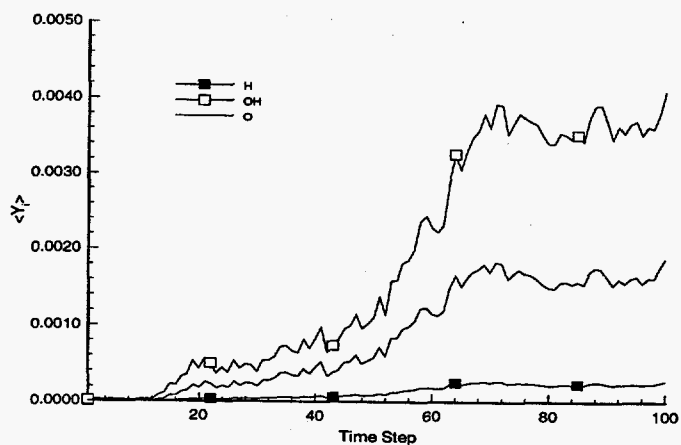**Figure 4. Average Mass Fraction of H, OH, O as Functions of Time**

Figure 5. Average Mass Fractions of H_2, CH_3, HO_2, CH_2O as Functions of Time
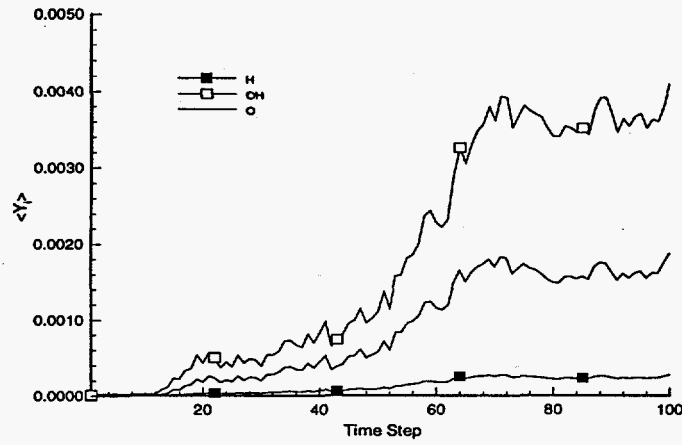
14

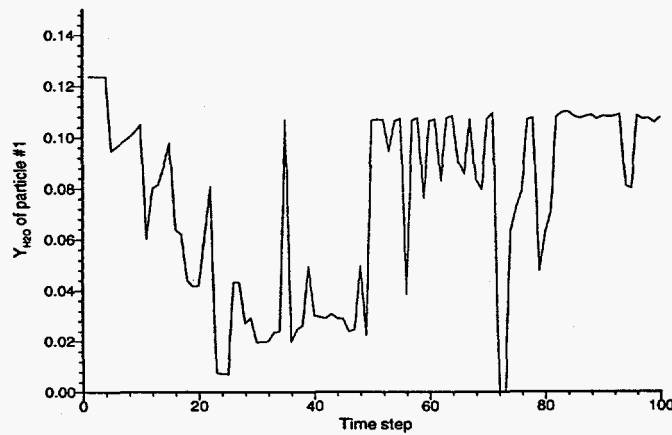**Figure 6.** Average Mass Fractions of HCO, H_2O_2, CH_3O as Functions of Time

Figure 7. The Mass Fraction of H_2O of the First Particle as a Function of Time
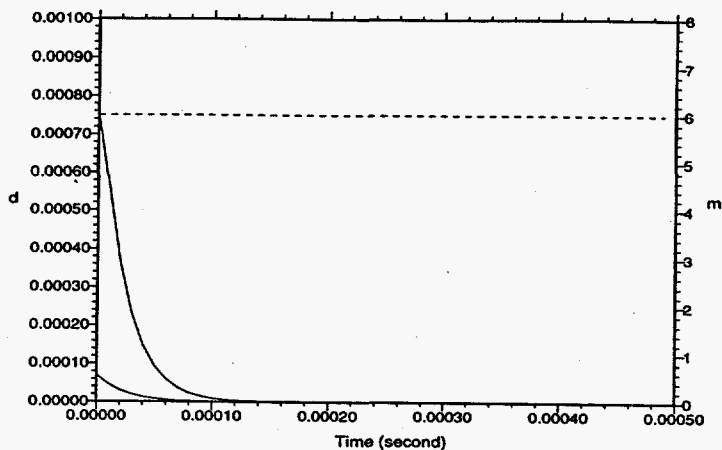
Figure 8. Changes of Distances of Particles from the Corresponding Manifold Points, d, Shown as Solid Lines, and the Dimension of the Manifolds, m, Shown as Dashed Lines, With Time. The Initial Dimensions are 6.
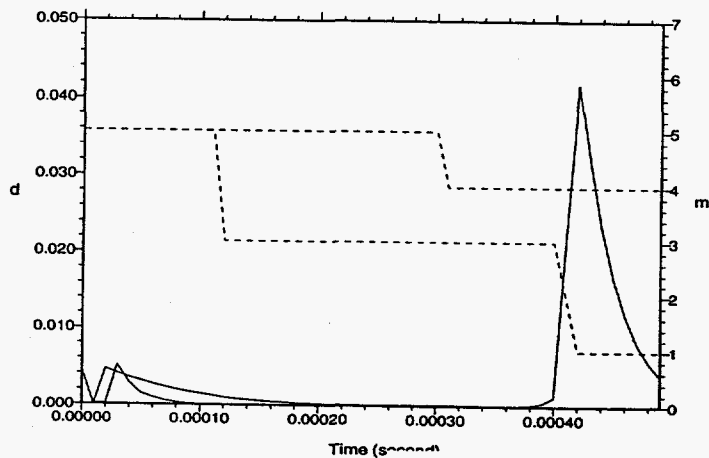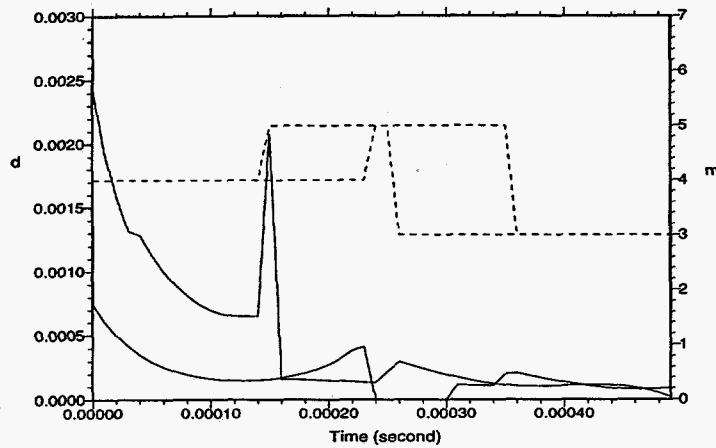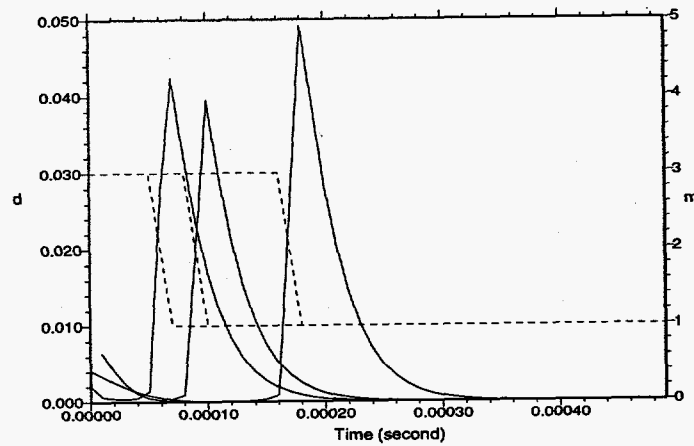

Figure 9. Changes of Distances of Particles from the Corresponding Manifold Points, d, Shown as Solid Lines, and the Dimension of the Manifolds, m, Shown as Dashed Lines, With Time. The Initial Dimensions are 5.
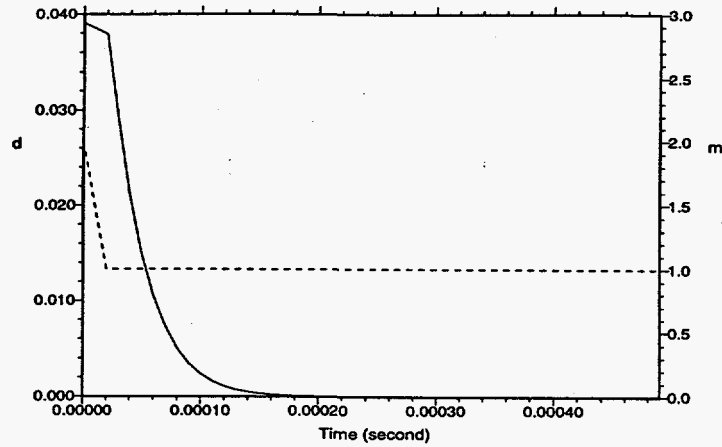
Figure 10. Changes of Distances of Particles from the Corresponding Manifold Points, d, Shown as Solid Lines, and the Dimension of the Manifolds, m, Shown as Dashed Lines, With Time. The Initial Dimensions are 4.

Figure 11. Changes of Distances of Particles from the Corresponding Manifold Points, d, Shown as Solid Lines, and the Dimension of the Manifolds, m, Shown as Dashed Lines, With Time. The Initial Dimensions are 3.

Figure 12. Changes of Distances of Particles from the Corresponding Manifold Points, d, Shown as Solid Lines, and the Dimension of the Manifolds, m, Shown as Dashed Lines, With Time. The Initial Dimensions are 2.
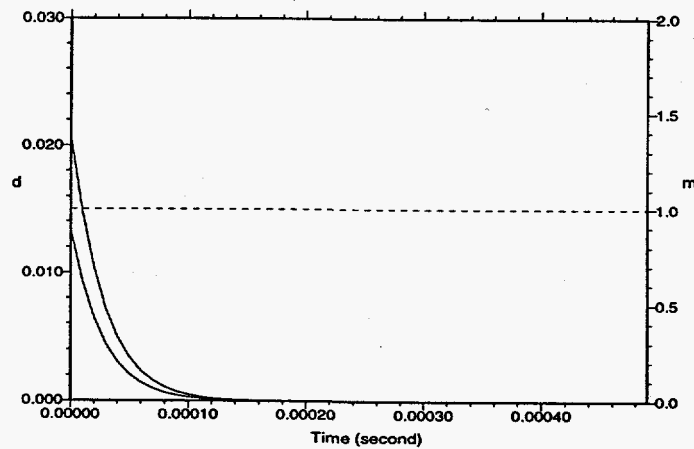

Figure 13. Changes of Distances of Particles from the Corresponding Manifold Points, d, Shown as Solid Lines, and the Dimension of the Manifolds, m, Shown as Dashed Lines, With Time. The Initial Dimensions are 1.
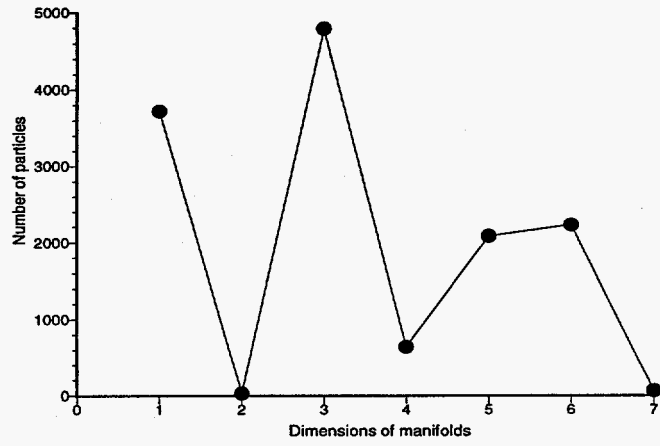
Figure 14. The Distribution of Particles as a Function of the Manifold Dimensions